Journal of Zhejiang University SCIENCE A
ISSN 1009-3095 (Print); ISSN 1862-1775 (Online)
www.zju.edu.cn/jzus; www.springerlink.com
E-mail: jzus@zju.edu.cn

Dynamic modelling and robust current control of wind-turbine driven DFIG during external AC voltage dip*

HU Jia-bing†, HE Yi-kang
(*Department of Electrical Engineering, Zhejiang University, Hangzhou 310027, China*)
†E-mail: emec_zju@zju.edu.cn

Received Sept. 12, 2005; revision accepted Dec. 25, 2005

Abstract: Doubly-Fed Induction Generator (DFIG), with vector control applied, is widely used in Variable-Speed Constant-Frequency (VSCF) wind energy generation system and shows good performance in maximum wind energy capture. But in two traditional vector control schemes, the equivalent stator magnetizing current is considered invariant in order to simplify the rotor current inner-loop controller. The two schemes can perform very well when the grid is in normal condition. However, when grid disturbance such as grid voltage dip or swell fault occurs, the control performance worsens, the rotor over current occurs and the Fault Ride-Through (FRT) capability of the DFIG wind energy generation system gets seriously deteriorated. An accurate DFIG model was used to deeply investigate the deficiency of the traditional vector control. The improved control schemes of two typical traditional vector control schemes used in DFIG were proposed, and simulation study of the proposed and traditional control schemes, with robust rotor current control using Internal Model Control (IMC) method, was carried out. The validity of the proposed modified schemes to control the rotor current and to improve the FRT capability of the DFIG wind energy generation system was proved by the comparison study.

Key words: Wind energy generation, Variable-Speed Constant-Frequency (VSCF), Doubly-Fed Induction Generator (DFIG), Fault Ride-Through (FRT), Internal Model Control (IMC)
doi:10.1631/jzus.2006.A1757 **Document code:** A **CLC number:** TM315; TM614

INTRODUCTION

Due to concerns about emissions from fossil fuels and the depletion of fossil fuel resources, renewable energy systems are becoming a topic of great interest and investment in the world. In particular, wind energy has been the subject of much recent research and development. In order to overcome the problems associated with fixed-speed wind-turbine system and to maximize the wind energy capture, many new wind farms will employ wind turbines based on Doubly-Fed Induction Generator (DFIG), which offer several advantages when compared with fixed speed generators including speed control, reduced flicker, and four-quadrant active and reactive power capabilities. These excellent merits are primarily achieved via control of a rotor side converter, which is typically rated at around 25% of the generator rating for a given rotor speed range of 0.75~1.25 p.u. under normal operation condition (Hansen *et al*., 2001; Muller *et al*., 2002). The schematic diagram of a DFIG generation system is shown in Fig.1.

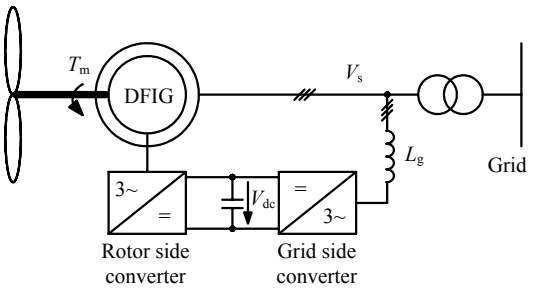

Fig.1 Doubly-Fed Induction Generator (DFIG) system

* Project (No.50577056) supported by the National Natural Science Foundation of China

The steady-state performance of DFIG wind turbine under normal grid condition is now well understood. However, the grid usually requires the wind generator to have Fault Ride-Through (FRT) capability during external AC fault. That means the generators are not allowed to disconnect from the network during disturbance such as voltage dip or swell. Because of the relatively small rating of the rotor side converter compared to the generator rating, it only provides partial control of the system. Therefore, the over current on the rotor side converter and subsequent over voltage on the converter DC link due to the excessive power coming from the rotor side during network disturbance easily occur and become two main concerns to system safety. Thus the main objectives of the control system during network fault are to limit the rotor over current and DC over voltage. Various types of control designs have been proposed for studying the behavior of DFIG based wind-turbine system during normal and fault AC grid conditions (HU *et al*., 2005; Morren and de Haan, 2005; Muller *et al*., 2002; Pena *et al*., 1996; Sun *et al*., 2004; 2005; Conraths, 2001). Most existing models widely use vector control based on Stator Flux Orientation (SFO). However, the existing control designs assume the stator voltage is ideal, i.e., the frequency and amplitude of the stator or grid voltage are constant and the dynamic characteristic of the stator magnetizing current is not considered (Pena *et al*., 1996; Sun *et al*., 2005; Conraths, 2001). Such a system can provide good dynamic response during normal operation condition but the performance may be degraded during AC voltage disturbance. System based on Stator Voltage Orientation (SVO) has also been used to control DFIG system (Muller *et al*., 2002; Anaya-Lara *et al*., 2004). In (Muller *et al*., 2002), SVO was proposed for controlling DFIG system under normal operation, but no detailed design of decoupling circuit was given and a constant stator voltage was assumed. In (Anaya-Lara *et al*., 2004), SVO control was used to investigate the fault current of DFIG. However, as no decoupling circuits were used, so that control response was inadequate during transient condition.

To reduce the over current and DC link over voltage to the rotor side converter, and to determine the DFIG stator voltage fault contribution and the power rating required for FRT capability and protection requirements, it is essential to propose a suitable control model and associated control strategies for DFIG system. This paper suggests two new-type SFO and SVO control models for DFIG system suitable for studying conditions with external network fault. Both model designs provide complete decoupling control, mainly introduced in the rotor voltage equations, and take the stator voltage variation transients into account. To verify the correctness and effectiveness of the new control designs in predicting dynamic behavior and in the evaluation of the impact of external network faults on DFIG and its rotor side converter, detailed simulation studies with robust current control using Internal Model Control (IMC) method, on a practical 2 MW DFIG wind-turbine system during normal and AC voltage dip conditions using two proposed control models and two conventional models, and assuming constant stator voltage, were carried out and compared. The effect of the control system on rotor fault current and converter DC link voltage was also illustrated by simulated results. The studies showed that the proposed models provide adequate control of the DFIG during AC voltage dips but that its capability was limited by the relatively small rating of the rotor side converter. The most critical situation was found under condition of high rotor speed and high stator output power, especially associated with the fault clearance effect. It was clearly shown that the two proposed control model designs are useful tools for DFIG fault studies and can be used to determine the required converter rating and protection device settings.

MATHEMATICAL MODEL OF DFIG

The equivalent circuit of a DFIG in an arbitrary reference frame rotating at synchronous angular speed ω_1 is shown in Fig.2.

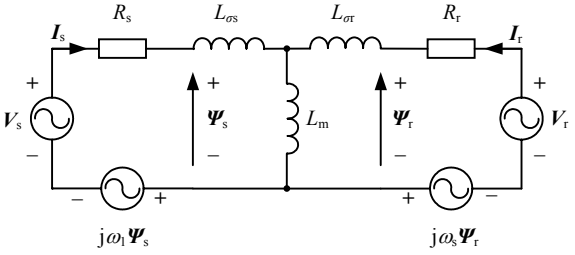

Fig.2 T representation of the DFIG equivalent circuit in the reference frame rotating at angular speed of ω_1

Fig.2 gives the stator and rotor fluxes $\boldsymbol{\Psi}_s$ and $\boldsymbol{\Psi}_r$ as

$$\begin{cases}\boldsymbol{\Psi}_s = L_s\boldsymbol{I}_s + L_m\boldsymbol{I}_r,\\ \boldsymbol{\Psi}_r = L_m\boldsymbol{I}_s + L_r\boldsymbol{I}_r,\end{cases} \tag{1}$$

and the stator and rotor voltages $\boldsymbol{V}_s$ and $\boldsymbol{V}_r$ as

$$\begin{cases}\boldsymbol{V}_s = R_s\boldsymbol{I}_s + \mathrm{d}\boldsymbol{\Psi}_s/\mathrm{d}t + \mathrm{j}\omega_1\boldsymbol{\Psi}_s,\\ \boldsymbol{V}_r = R_r\boldsymbol{I}_r + \mathrm{d}\boldsymbol{\Psi}_r/\mathrm{d}t + \mathrm{j}(\omega_1-\omega_r)\boldsymbol{\Psi}_r,\end{cases} \tag{2}$$

where, R_s and R_r are stator and rotor resistance respectively, $L_s=L_{\sigma s}+L_m$ and $L_r=L_{\sigma r}+L_m$ are total self-inductance of stator and rotor winding respectively, $L_{\sigma s}$, $L_{\sigma r}$ and L_m are stator and rotor leakage inductance and mutual inductance respectively, ω_1 is synchronous angular speed, ω_r is rotor angular speed, $\omega_s=\omega_1-\omega_r$ is slip angular speed.

The active and reactive output power from DFIG are represented respectively by

$$\begin{cases}P = -3\,\mathrm{Re}[\boldsymbol{V}_s\boldsymbol{I}_s^*]/2,\\ Q = -3\,\mathrm{Im}[\boldsymbol{V}_s\boldsymbol{I}_s^*]/2.\end{cases} \tag{3}$$

The equivalent stator magnetizing current $\boldsymbol{I}_{mo}$ is defined as

$$\boldsymbol{\Psi}_s = L_s\boldsymbol{I}_s + L_r\boldsymbol{I}_r = L_s\boldsymbol{I}_{mo}. \tag{4}$$

From Eq.(4),

$$\boldsymbol{I}_{mo} = L_s\boldsymbol{I}_s/L_m + \boldsymbol{I}_r, \tag{5}$$

$$\boldsymbol{I}_s = L_m(\boldsymbol{I}_{mo} - \boldsymbol{I}_r)/L_s, \tag{6}$$

$$\boldsymbol{\Psi}_r = L_m^2\,\boldsymbol{I}_{mo}/L_s + \sigma L_r\,\boldsymbol{I}_r, \tag{7}$$

where $\sigma = 1 - L_m^2/(L_rL_s)$.

Substituting $\boldsymbol{\Psi}_s$ in Eq.(4), $\boldsymbol{I}_s$ in Eq.(6) and $\boldsymbol{\Psi}_r$ in Eq.(7) into Eq.(2) yields the stator and rotor voltages in the synchronous *d-q* reference frame as

$$\begin{cases}\boldsymbol{V}_s = R_s\boldsymbol{I}_s + L_m\cdot\mathrm{d}\boldsymbol{I}_{mo}/\mathrm{d}t + \mathrm{j}\omega_1\boldsymbol{\Psi}_s,\\ \boldsymbol{V}_r = R_r\boldsymbol{I}_r + \sigma L_r\cdot\mathrm{d}\boldsymbol{I}_r/\mathrm{d}t + (L_m^2/L_s)\cdot\mathrm{d}\boldsymbol{I}_{mo}/\mathrm{d}t + \mathrm{j}\omega_s\boldsymbol{\Psi}_r.\end{cases} \tag{8}$$

TRADITIONAL VECTOR CONTROLS AND THEIR LIMITATIONS

If the stator voltage $\boldsymbol{V}_s$ and flux $\boldsymbol{\Psi}_s$ in Eq.(8) are assumed to be constant, $\mathrm{d}\boldsymbol{I}_{mo}/\mathrm{d}t=0$, whereas the four-order voltage equation is degraded into a two-order one

$$\boldsymbol{V}_r = R_r\boldsymbol{I}_r + \sigma L_r\cdot\mathrm{d}\boldsymbol{I}_r/\mathrm{d}t + \mathrm{j}\omega_s\boldsymbol{\Psi}_r. \tag{9}$$

Eq.(9) is the basis for designing the current inner loop controllers in the traditional vector control strategies, where $R_r\boldsymbol{I}_r+\sigma L_r\cdot\mathrm{d}\boldsymbol{I}_r/\mathrm{d}t$ depends on PI parameter design, and $\mathrm{j}\omega_s\boldsymbol{\Psi}_r$ is used to compensate for the elimination of the cross coupling.

In order to obtain robust current control, the IMC principle below can be applied for designing the PI parameters (Harnefors and Nee, 1998)

$$k_p = \alpha_c\sigma L_r,\ k_i = \alpha_c R_r, \tag{10}$$

where α_c is the bandwidth of the current control loop, k_p is the proportional gain, and k_i is the integral gain.

Whether SFO or SVO is adopted, Eq.(9) should be separated into *d-q* components

$$\begin{cases}V_{rd} = R_rI_{rd} + \sigma L_r\cdot\mathrm{d}I_{rd}/\mathrm{d}t - \omega_s\Psi_{rd},\\ V_{rq} = R_rI_{rq} + \sigma L_r\cdot\mathrm{d}I_{rq}/\mathrm{d}t + \omega_s\Psi_{rq}.\end{cases} \tag{11}$$

According to Eq.(11), the two control strategies have the same current control loop structure. However, their power control loops have some differences, which result from the fact that *d-q* axes in different vector orientations represent different power axes, respectively. For example, in SFO the stator output active and reactive power can be independently controlled by controlling the rotor *q*- and *d*-axis currents respectively, represented by Eq.(11); while in SVO the *d*- and *q*-axis currents refer to the stator output active and reactive power components respectively, represented by Eq.(12).

Neglecting the stator resistive voltage drop, the stator output active and reactive powers with SFO are expressed as

$$\begin{cases} P \approx 1.5\omega_1 L_m \Psi_s I_{rq} / L_s, \\ Q \approx 1.5\omega_1 L_m^2 \Psi_s (I_{rd} - \Psi_s / L_m) L_s^{-1}. \end{cases} \quad (12)$$

From Eq.(11) and Eq.(12), DFIG control based on traditional SFO can be designed as shown in Fig.3.

Similarly, neglecting the stator resistive voltage drop, with SVO the stator output active and reactive powers are represented by

$$\begin{cases} P \approx 1.5 L_m V_s I_{rd} / L_s, \\ Q \approx -1.5 V_s (V_s / \omega_1 + L_m I_{rq}) L_s^{-1}. \end{cases} \quad (13)$$

Based on Eq.(11) and Eq.(13), DFIG control with SVO can be designed as shown in Fig.4.

From the analysis above, the traditional control designs assume the stator voltage is ideal, such system can provide good dynamic response during

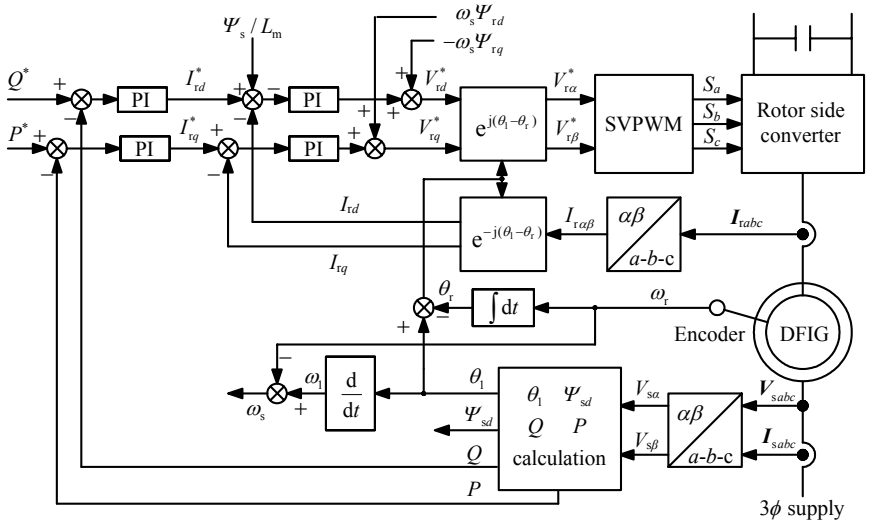

Fig.3 Diagram of the traditional stator flux vector oriented control

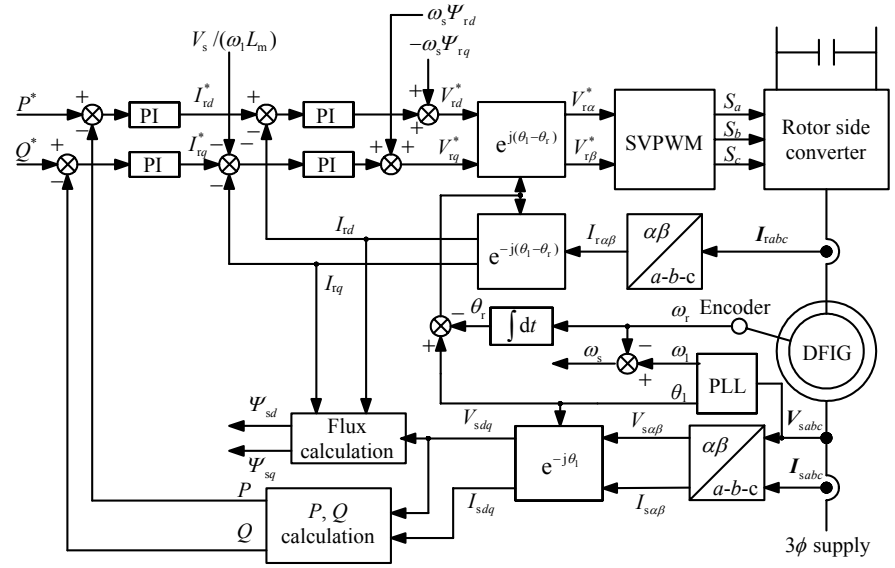

Fig.4 Diagram of the traditional stator voltage vector oriented control

normal operation conditions, although the performance may be degraded during AC voltage disturbance. Therefore, in order to improve the FRT capability of DFIG during external network fault, it is essential to use the proposed suitable control models and associated control strategies for DFIG system.

NEW DFIG CONTROL MODELS WITH GRID VOLTAGE DYNAMICS CONSIDERED

To design a control system to provide full decoupling and good response under stator voltage variation, it is necessary to consider the stator magnetizing current dynamics $\boldsymbol{I}_{\mathrm{mo}}$.

When stator voltage $\boldsymbol{V}_s$ and flux $\boldsymbol{\Psi}_{\mathrm{s}}$ are assumed to be variable, it can be obtained from Eq.(8) that

$$\mathrm{d}\boldsymbol{I}_{\mathrm{mo}}/\mathrm{d}t=(\boldsymbol{V}_{\mathrm{s}}-R_{\mathrm{s}}\boldsymbol{I}_{\mathrm{s}}-\mathrm{j}\omega_{\mathrm{l}}\boldsymbol{\Psi}_{\mathrm{s}})/L_{\mathrm{m}}. \tag{14}$$

Substituting $\mathrm{d}\boldsymbol{I}_{\mathrm{mo}}/\mathrm{d}t$ in Eq.(14) into Eq.(8) yields rotor voltage

$$\begin{aligned}\boldsymbol{V}_{\mathrm{r}}=&R_{\mathrm{r}}\boldsymbol{I}_{\mathrm{r}}+\sigma L_{\mathrm{r}}\cdot\mathrm{d}\boldsymbol{I}_{\mathrm{r}}/\mathrm{d}t+\mathrm{j}\omega_{\mathrm{s}}\boldsymbol{\Psi}_{\mathrm{r}}\\&+L_{\mathrm{m}}(\boldsymbol{V}_{\mathrm{s}}-R_{\mathrm{s}}\boldsymbol{I}_{\mathrm{s}}-\mathrm{j}\omega_{\mathrm{l}}\boldsymbol{\Psi}_{\mathrm{s}})/L_{\mathrm{s}}\end{aligned} \tag{15}$$

used as basis for improved controller designs. Comparison of Eq.(15) with Eq.(8) shows that the extra term on $\boldsymbol{V}_{\mathrm{r}}$ presented in Eq.(15) considers the variation of stator magnetizing current and provides complete decoupling of the system so that Eq.(15) represents the DFIG system under both normal and AC fault conditions and can be used to design the required control system.

With SFO, $\Psi_{sd}=|\boldsymbol{\Psi}_{\mathrm{s}}|$, $\Psi_{sq}=0$ and $\boldsymbol{\Psi}_{\mathrm{s}}=\Psi_{sd}+\mathrm{j}\cdot0$, so Eq.(15) can be represented as

$$\begin{cases}V_{\mathrm{r}d}=R_{\mathrm{r}}I_{\mathrm{r}d}+\sigma L_{\mathrm{r}}\cdot\mathrm{d}I_{\mathrm{r}d}/\mathrm{d}t-\omega_{\mathrm{s}}\Psi_{\mathrm{r}q}\\\qquad+L_{\mathrm{m}}(V_{sd}-R_{\mathrm{s}}I_{\mathrm{s}d})/L_{\mathrm{s}},\\V_{\mathrm{r}q}=R_{\mathrm{r}}I_{\mathrm{r}q}+\sigma L_{\mathrm{r}}\cdot\mathrm{d}I_{\mathrm{r}q}/\mathrm{d}t+\omega_{\mathrm{s}}\Psi_{\mathrm{r}d}\\\qquad+L_{\mathrm{m}}(V_{sq}-R_{\mathrm{s}}I_{\mathrm{s}q}-\omega_{\mathrm{l}}\Psi_{\mathrm{s}d})/L_{\mathrm{s}}.\end{cases} \tag{16}$$

The improved control diagram is quite similar to that in Fig.3, except for that the items $\omega_{\mathrm{s}}\Psi_{rd}$ and $-\omega_{\mathrm{s}}\Psi_{rq}$ are replaced by $\omega_{\mathrm{s}}\Psi_{rd}+L_{\mathrm{m}}(V_{sq}-R_{\mathrm{s}}I_{sq}-\omega_{\mathrm{l}}\Psi_{sd})/L_{\mathrm{s}}$ and $-\omega_{\mathrm{s}}\Psi_{rq}+L_{\mathrm{m}}(V_{sd}-R_{\mathrm{s}}I_{sd})/L_{\mathrm{s}}$, respectively.

With SVO, $V_{sd}=|\boldsymbol{V}_{\mathrm{s}}|$, $V_{sq}=0$ and $\boldsymbol{V}_{\mathrm{s}}=V_{sd}+\mathrm{j}\cdot0$, so Eq.(15) can be expressed as

$$\begin{cases}V_{\mathrm{r}d}=R_{\mathrm{r}}I_{\mathrm{r}d}+\sigma L_{\mathrm{r}}\cdot\mathrm{d}I_{\mathrm{r}d}/\mathrm{d}t-\omega_{\mathrm{s}}\Psi_{\mathrm{r}q}\\\qquad+L_{\mathrm{m}}(V_{sd}-R_{\mathrm{s}}I_{\mathrm{s}d}+\omega_{\mathrm{l}}\Psi_{\mathrm{s}q})/L_{\mathrm{s}},\\V_{\mathrm{r}q}=R_{\mathrm{r}}I_{\mathrm{r}q}+\sigma L_{\mathrm{r}}\cdot\mathrm{d}I_{\mathrm{r}q}/\mathrm{d}t+\omega_{\mathrm{s}}\Psi_{\mathrm{r}d}\\\qquad+L_{\mathrm{m}}(-R_{\mathrm{s}}I_{\mathrm{s}q}-\omega_{\mathrm{l}}\Psi_{\mathrm{s}d})/L_{\mathrm{s}}.\end{cases} \tag{17}$$

The improved control diagram is quite similar to that in Fig.4, except for that the items $\omega_{\mathrm{s}}\Psi_{rd}$ and $-\omega_{\mathrm{s}}\Psi_{rq}$ are replaced by $\omega_{\mathrm{s}}\Psi_{rd}+L_{\mathrm{m}}(-R_{\mathrm{s}}I_{sq}-\omega_{\mathrm{l}}\Psi_{sd})/L_{\mathrm{s}}$ and $-\omega_{\mathrm{s}}\Psi_{rq}+L_{\mathrm{m}}(V_{sd}-R_{\mathrm{s}}I_{sd}+\omega_{\mathrm{l}}\Psi_{sq})/L_{\mathrm{s}}$, respectively.

SIMULATION INVESTIGATION

In order to verify the FRT capability of the proposed modified DFIG models and associated control strategies, simulations for DFIG generation were carried out using Matlab/Simulink. DFIG is rated at 2 MW and its parameters are given in Table 1. Rotor and grid side converters were represented using the average VSC models (Thomas *et al*., 2001). The normal DC link voltage was set at 1200 V with the DC capacitance being 16 mF. The results shown here were for conditions where the dip in the stator voltage was about 67%, which is approximately a common value when voltage dip at the point of common coupling was around 85% (National Grid Transco, 2004).

Table 1 Parameters of the simulated DFIG

Parameter	Value
Rated power	2 MW
Stator voltage	690 V
Stator/rotor turns ratio	0.38
R_{s}	0.0108 p.u.
R_{r}	0.0121 p.u. (referred to the stator)
L_{m}	3.362 p.u.
$L_{\sigma\mathrm{s}}$	0.102 p.u.
$L_{\sigma\mathrm{r}}$	0.11 p.u. (referred to the stator)
Lumped inertia const.	3

First, simulations under normal conditions with various rotor active and reactive current steps are shown in Fig.5a and Fig.5b for SFO and SVO respectively. The same parameters for the current and

DC voltage regulators were used for the two designs. During the simulation, the rotor speed was kept at 0.8 p.u. as rotor speed variation was slow due to the large inertia of the turbine/generator system. Besides the active and reactive powers, the voltage and current waveforms shown are also in per unit values. Fig.5a shows that the rotor *d*-axis current reference was step changed from 0.06 p.u. to 0.25 p.u. at 1.5 s while for the *q*-axis current reference, a step from 0.35 p.u. to 0.55 p.u. was applied at 1.7 s. This corresponds to the changes of reactive power from 0.3 p.u. to 0 p.u. at 1.5 s and active power from 0.35 p.u. to 0.55 p.u. at 1.7 s respectively. For the results shown in Fig.5b with SVO, similar rotor current steps were applied to get the same stator active and reactive power changes as shown in Fig.5a. Comparison of the system responses shown in Fig.5a and Fig.5b showed obviously that the two control designs have almost identical stator and rotor current waveforms respectively. The responses during various rotor current steps are satisfactory for both control designs.

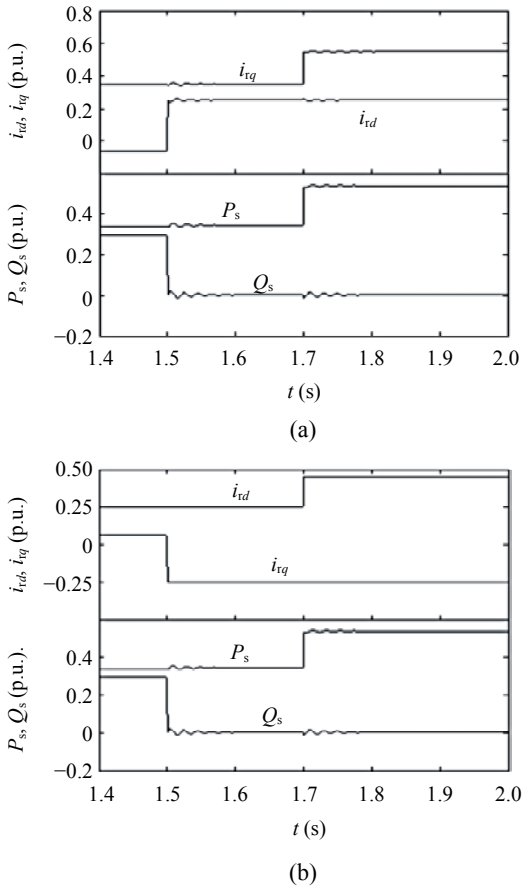

Fig.5 Simulation results of the proposed control schemes under normal grid condition. (a) Stator Flux Orientation (SFO); (b) Stator Voltage Orientation (SVO)

It was found that during AC voltage dip, the most critical situation when both rotor speed and stator active power output were at their maximum values before the AC fault, as higher rotor speed generates higher voltage on the rotor side. A higher voltage from the rotor side converter is required during AC voltage dip for adequate control. However the voltage that can be generated by the rotor side converter is limited which is one of the main causes of DFIG FRT problem. Higher stator active power output accompanies higher current and is more likely to induce over current during voltage dips. Therefore, in the following studies, the rotor speed and stator active power output was set at 1.2 p.u. and 1.0 p.u. (2 MW), respectively.

Besides, fault clearance time has great effect on the FRT capability of the DFIG system with stability considered during voltage dips, although grid fault occurrence time is meaningless to it. The simulation results with different fault clearance time and with SVO applied after grid voltage dips are demonstrated in Fig.6, the fault occurred at 1.5 s, which lowered the stator voltage to 0.5 of its nominal value, and cleared at different time. It is concluded that when the fault duration time is just even times the half grid period (0.01 s), the peak stator fluxes after fault clearance are distinctly smaller, including labels 2, 5, 8, compared with those when the fault duration time is just odd times the half grid period, including labels 1, 3, 4, 6, 7, 9. As a result, the latter need relatively larger rotor magnetizing control current. Hence, to determine the required converter rating and protection device

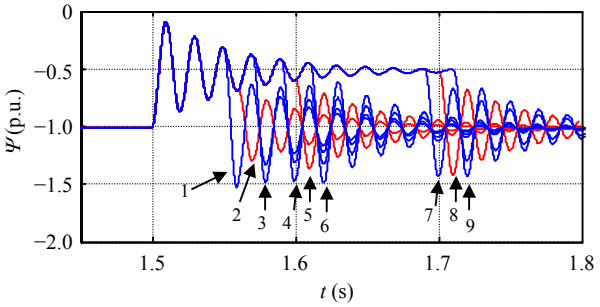

Fig.6 *q*-axis stator flux with SVO at different fault clearance time of grid voltage
(1: 0.05 s; 2: 0.06 s; 3: 0.07 s; 4: 0.09 s; 5: 0.10 s; 6: 0.11 s; 7: 0.19 s; 8: 0.20 s; 9: 0.21 s)

settings during FRT operations, it is necessary to introduce the critical situations among different grid fault clearance time.

During the simulation, the fault occurred at 1.5 s, which lowered the stator voltage to 0.67 of its nominal value, and cleared at 1.7 s. For comparison, Fig.7 shows the simulated results with the conventional and the proposed SFO designs for the same operating conditions, and results for the conventional and the proposed SVO designs are shown in Fig.8.

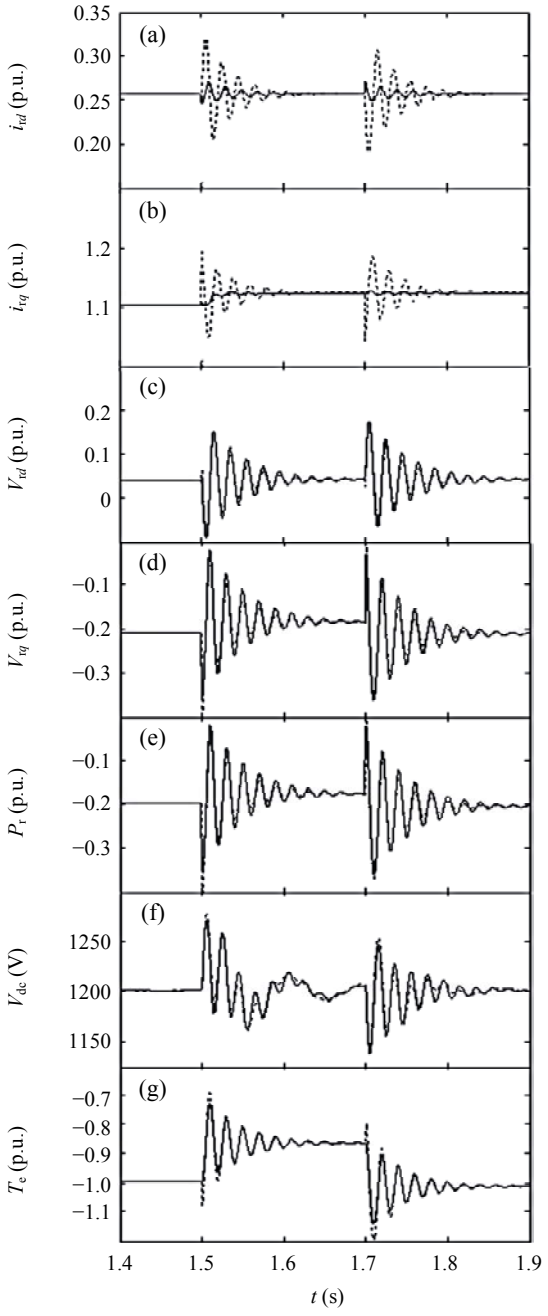

Fig.7 Comparison of the response between the traditional and the proposed stator flux vector oriented control under the grid voltage dip fault (----- the traditional control; —— the proposed control)

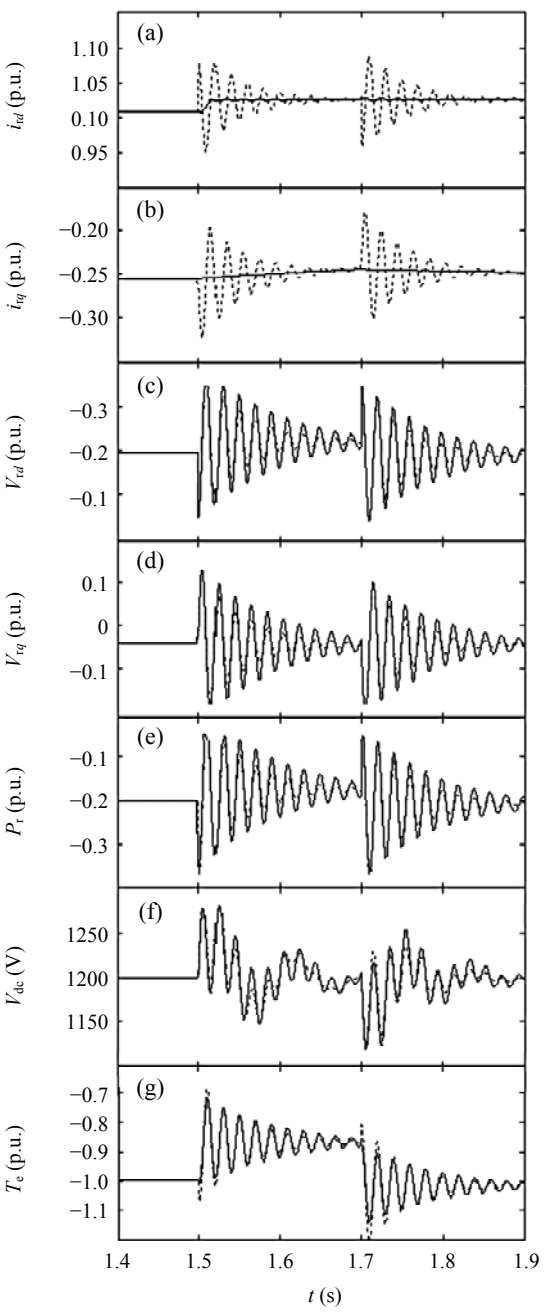

Fig.8 Comparison of the response between the traditional and the proposed stator voltage vector oriented control under the grid voltage dip fault (----- the traditional control; —— the proposed control)

Comparison of Fig.7 and Fig.8 showed that the two control designs again resulted in almost identical waveforms during AC voltage dip. According to (a) (b), the proposed control designs resulted in much smaller rotor over currents than the conventional design, indicating that the proposed control designs could provide adequate control on over current of both the rotor and the rotor side converter. (c) (d) showed that the rotor voltage with the proposed control designs is somewhat larger than that with the conventional design, because the proposed design takes into account the stator magnetizing current dynamics, indicating that effective control on the rotor current is achieved by increasing rotor side voltage. According to (e) (f) (g), the proposed control designs could not decrease the active power absorbed in the rotor side converter so that they contribute little to the DC voltage, but reduce peak electric torque.

CONCLUSION

Two control designs suitable for studying the DFIG behaviors during external network fault have been proposed and validated by simulations. One design is based on stator flux orientation and the other is based on stator voltage orientation. Both designs take into account the dynamics of stator voltage variation and, thus, provide full decoupling of the system. It has been shown that the proposed control designs provide adequate control of the DFIG during AC voltage dips although its capabilities are limited by the relatively small rating of the rotor side converter compared to the DFIG. The most critical situation occurs under conditions of high rotor speed and high stator output power. The two proposed control designs provide helpful tools for DFIG faults studies and can be used to determine the required converter rating and protection device settings.

References

Anaya-Lara, O., Cartwright, P., Ekanayake, J.B., 2004. Electrical Stability of Large Wind Farms—Grid Connections and Modeling. Proc. 2004 AWEA Conference.

Conraths, H.J., 2001. Rotor Control Generator System for Wind Energy Applications. Proc. EPE2001. Graz, Australia.

Hansen, L.H., Helle, L., Blaabjerg, F., Rithite, E., Munk-Nielsen, S., Bindner, H., Sørensen, P., Bak-Jensen, B., 2001. Conceptual Survey of Generators and Power Electronics for Wind Turbines. Tech. Rep. Riso-R1205 (EN), Riso Nat. Lab., Roskilde, Demark.

Harnefors, L., Nee, H.P., 1998. Model-based current control of AC machines using the internal model control method. *IEEE Trans. Ind. Appl*., **34**(1):133-141. [doi:10.1109/28.658735]

Hu, J.B., He, Y.K., Liu, Q.H., 2005. Optimized active power reference based maximum wind energy tracking control strategy. *Automation of Electric Power Systems*, **29**(24): 32-38 (in Chinese).

Morren, J., de Haan, S.W.H., 2005. Ridethough of wind turbines with doubly-fed induction generator during a volage dip. *IEEE Transactions on Energy Conversion*, **20**(2):435-441. [doi:10.1109/TEC.2005.845526]

Muller, S., Deicke, M., de Doncker, R.W., 2002. Doubly fed induction generator system for wind turbines. *IEEE Industry Application Magazine*, **8**(3):26-33. [doi:10.1109/2943.999610]

National Grid Transco, 2004. Appendix 1: Extracts from the Grid Code—Connection Conditions. Available at http://www.nationalgrid.com

Pena, R., Clare, J.C., Asher, G.M., 1996. Doubly fed induction generator using back-to-back PWM converters and its application to variable-speed wind-energy generation. *IEEE Proceedings of Electric Power Applications*, **143**(3): 231-241. [doi:10.1049/ip-epa:19960288]

Sun, T., Chen, Z., Blaabjerg, F., 2004. Voltage Recovery of Grid-connected Wind Turbines with DFIG after a Short-circuit Fault. 35th Annual IEEE Power Electronics Specialist Conference, p.1991-1997.

Sun, T., Chen, Z., Blaabjerg, F., 2005. Transient stability of DFIG wind turbines at an external short-circuit fault. *Wind Energy*, **8**(3):345-360. [doi:10.1002/we.164]

Thomas, J.L., Poullain. S., Benchaib, A., 2001. Analysis of a Robust DC-bus Voltage Control System for a VSC-transmission Scheme. IEEE Proc. of the 7th International Conference on AC-DC Power Transmission. London, p.119-124.